Biomedicine & Pharmacotherapy 153 (2022) 113380

Contents lists available at ScienceDirect

Biomedicine & Pharmacotherapy

journal homepage: www.elsevier.com/locate/biopha

Farnesoid X receptor activation by the novel agonist TC-100 (3α, 7α, 11β-Trihydroxy-6α-ethyl-5β-cholan-24-oic Acid) preserves the intestinal barrier integrity and promotes intestinal microbial reshaping in a mouse model of obstructed bile acid flow

M. Marzano [a,1], Bruno Fosso [a,1], C. Colliva [c], E. Notario [b], D. Passeri [c], M. Intranuovo [b], A. Gioiello [d], L. Adorini [e], G. Pesole [a,b], R. Pellicciari [c], A. Moschetta [f], R.M. Gadaleta [f,*]

[a] Institute of Biomembranes, Bioenergetics and Molecular Biotechnology (IBIOM), National Council of Research (CNR), Via Amendola, 70126 Bari, Italy
[b] Department of Biosciences, Biotechnology and Biopharmaceutics, University of Bari, via Orabona 125, 70125 Bari, Italy
[c] TES Pharma S.r.l., Via Palmiro Togliatti 22bis, I-06073 Loc. Terrioli, Corciano, Perugia, Italy
[d] Department of Pharmaceutical Science, University of Perugia, via del Liceo, 1, 06123 Perugia, Italy
[e] Intercept Pharmaceuticals, San Diego, CA, USA
[f] Department of Interdisciplinary Medicine, University of Bari, Piazza Giulio Cesare 11, 70100 Bari, Italy

ARTICLE INFO

Keywords:
Bile acids
Gut microbiota
Akkermansia muciniphila
Intestinal Barrier Integrity
Gut-liver axis

ABSTRACT

The intestinal tract hosts the gut microbiota (GM), actively shaping health. Bile acids(BAs) are both digestive and signaling molecules acting as hormones via the activation of farnesoid X receptor (FXR). Obstruction of bile flow initiates a cascade of pathological events ultimately leading to intestinal mucosal injury. Administration of BAs in models of obstructed bile flow counteracts these detrimental effects. Objective of this study was to investigate the effects of the novel FXR agonist 3α, 7α, 11β-Trihydroxy-6α-ethyl-5β-cholan-24-oic Acid (TC-100) on intestinal mucosa integrity and cecal microbiome composition after surgical bile duct ligation (BDL), a rodent model causing bile flow obstruction.

Pharmacological FXR activation was accomplished by daily oral gavage with TC-100 for 5 days. 2 days after treatment initiation, BDL was performed. BAs measurement was carried out and the 16S rDNA (V5-V6 hypervariable regions) extracted from the cecal content was sequenced.

TC-100 activates Fxr in the gut-liver axis and this translated into a significant reduction of serum and bile BA pool size with a shift to a more hydrophilic composition, while signs of intestinal mucosal damage were prevented. Firmicutes:Bacteroidota ratio progressively increased from Sham Operated (SO) mice to TC-100-treated mice. LEfSe analysis showed that Verrucomicrobia, and particularly *Akkermansia muciniphila* (*Amuc*) increasingly recognized for improving gut homeostasis and immune functions, were strongly associated to TC-100-treated mice. Intriguingly, *Amuc* abundance was also negatively associated to cholic acid levels.

Collectively, these data indicate that intestinal FXR activation by TC-100 prevents early signs of intestinal mucosal damage by modulating BA homeostasis and GM composition.

Abbreviation: Amuc, *Akkermansia muciniphila*; Ang1, angiogenin 1; ASV, Amplicon Sequence Variants; BA, bile acid; BDL, bile duct ligation; BSH, bile salt hydrolase; CA, cholic acid; Cldn, Cloudin; Cyp7a1, Cholesterol 7 alpha-hydroxylase or Cytochrome P450 Family 7 Subfamily A Member 1; DCA, deoxycholic acid; ddPCR, Droplet digital PCR; FGF15/19, fibroblast growth factor 15/19; FGFR4, fibroblast growth factor receptor 4; FXR, farnesoid X receptor; GCA, glycol-cholic acid; GM, gut microbiota; H&E, Hematoxylin and Eosin; HI, hydrophobicity index; LDA, linear discriminant analysis; MC, methyl-cellulose; MCA, muricholic acid; KLB, klotho-beta; OCA, obeticholic acid; qRT-PCR, quantitative real time polymerase chain reaction; SEM, standard error of the mean; Shp, small heterodimer partner; SO, sham operated; Tau-α-MCA, tauro-α-MCA; Tau-CA, taurocholic acid; Tau-MCA, tauro-muricholic acid; TC-100, 3α, 7α, 11β-Trihydroxy-6α-ethyl-5β-cholan-24-oic Acid; Tau-CDCA, tauro-chenodeoxycholic acid; Tau-DCA, tauro-deoxycholic acid; Tau-UDCA, tauro-ursodeoxycholic acid; UDCA, ursodeoxycholic acid; UPLC-MS, Ultra Performance Liquid Chromatography-Mass Spectrometry system; WGCNA, Weighted Gene Correlation Network Analysis; WT, wild type.

* Correspondence to: RM Gadaleta, Department of Interdisciplinary Medicine, University of Bari "Aldo Moro", Piazza Giulio Cesare n.11, 70100 Bari, Italy.
E-mail address: raffaella.gadaleta@uniba.it (R.M. Gadaleta).

[1] Shared authorship.

https://doi.org/10.1016/j.biopha.2022.113380
Received 21 April 2022; Received in revised form 21 June 2022; Accepted 6 July 2022
Available online 19 July 2022

1. Introduction

The human intestinal tract hosts a huge variety of microorganisms actively shaping human health, collectively named gut microbiota (GM). Intestinal bacteria could be divided in six main phyla: Firmicutes, Bacteroidota, Proteobacteria, Actinobacteria, Fusobacteria, and Verrucomicrobia [1], with Firmicutes and Bacteroidota making up to 90 % of the total bacterial composition. The host and its resident microbiota are constantly engaged in a dynamic bidirectional communication governed by complex codes. A very sophisticated balance regulates host's health and diseases. While an excessive number or imbalance of resident bacteria may contribute to the onset of inflammatory or autoimmune conditions, a reduced variety of microorganisms decreases the ability of the host to resist infections, assimilate nutrients or perform a wide range of metabolic activities [2]. The composition of the GM is influenced by multiple factors such as lifestyle, nutrition, drug administration, genetic and epigenetic factors. In homeostasis, the GM efficiently performs his specific functions: maintaining its own balance by regulating the integrity of the intestinal epithelium, peristalsis and by training and supporting the intestinal resident immune system. Perturbation of this balance, also known as dysbiosis, increases susceptibility to infections and can prime aberrant immune responses, thereby playing a role in the pathogenesis of diseases of the gut-liver axis [3], inflammatory [4] and autoimmune diseases [5].

Bile acids (BA) are amphypathic molecules synthesized from cholesterol in the liver and released in the intestine after a meal to aid the absorption of lipids and liposoluble vitamins. Primary BAs act as signaling hormones via binding to their cognate Farnesoid X receptor (FXR) [6–8]. Once activated by BAs, FXR primes the transcription of genes involved in BA synthesis, transport and metabolism in the gut-liver axis. In particular, via a negative feedback loop, activated FXR inhibits BA hepatic synthesis, via the transactivation of its intestinal target Fibroblast growth factor 15/19 (FGF15/19 in mouse and human, respectively) [9] that travels back to the liver, binds to its cognate co-receptor fibroblast growth receptor 4 (FGFR4)-Klotho-beta (KLB) and initiate a phosphorylation signaling cascade resulting in the inhibition of the rate-limiting enzyme of BA synthesis, Cholesterol 7 alpha-hydroxylase (CYP7A1) [10–13]. An altered BA signaling in the gut-liver axis, and in particular abnormally elevated BA levels, have been associated with a wide range of diseases of the gut-liver axis [14–18]. Besides acting as digestive metabolites and signaling molecules via FXR, BAs also interact with the gut microbial community and affect the integrity of the intestinal epithelial barrier. Obstruction of bile flow, as it occurs in bile duct obstruction, leads to abnormal hepatic BA accumulation and abrogates intestinal FXR signaling [19]. Surgical ligation of the common bile duct (BDL) is a commonly used model for studying the underlying molecular and cellular events induced by arrest of bile flow in the gut-liver axis. BDL also devoids the intestine of BAs, an event that negatively influences the intestinal microbial community and cause mucosal injury [20]. Administration of BAs [21–24] to both rodents and humans in conditions of biliary obstruction as well as FXR activation [19] or FGF19 [25] administration in the presence of intestinal inflammatory triggers, counteract intestinal mucosal damage and bacterial overgrowth and translocation.

The GM and BAs dynamically interact with each other. BA flow along the intestine controls bacterial overgrowth and protects against inflammation while intestinal microorganisms affect BA metabolism [26,27], mainly via the action of the microbial bile salt hydrolase (BSH) enzymes that catalyze BA deconjugation [28,29]. BSH activity has been found in all major bacterial groups and archaeal species in the human gut [30], including members of *Lactobacilli* [31,32], *Bifidobacteria* [33–35] and *Clostridium* [36,37]. The novel FXR agonist 3α, 7α, 11β-Trihydroxy-6α-ethyl-5β-cholan-24-oic Acid (TC-100) is a novel semi-synthetic BA [38]. Intriguingly, TC-100 displays a peculiar pharmacological profile combining the ability to bind and regulate intestinal FXR *in vivo* with high potency and selectivity together with hydrophilic BA properties similar to ursodeoxycholic acid (UDCA) [38]. Compared to the most well studied and characterized bile acid-derivative obeticholic acid (OCA), TC-100 exhibits higher water solubility, poor detergent properties and absence of cytotoxicity [39]. The aim of this study is to investigate the effect of TC-100 on the intestinal mucosa and GM composition, in relation to BA pool size and composition, in a mouse model of obstructed bile flow.

2. Material and methods

2.1. Animals

Wild-type (WT) C57BL/6J male mice (9–12 weeks old) were obtained from Charles River Laboratories (Calco, Lecco, Italy). Mice were fed ad libitum and housed in a temperature and light-controlled room. The Ethical Committee of the University of Bari and Fondazione "Mario Negri" Sud approved this experimental set-up, which was also certified by the Italian Ministry of Health in accordance with internationally accepted guidelines for animal care (protocol code 17198-X/10 date 7 March 2014).

2.2. Pharmacological activation of FXR and bile duct ligation

TC-100 was kindly provided by TES Pharma. Pharmacological activation of FXR was accomplished by daily oral gavage with 10 mg/kg/day of TC-100 (n = 6) or vehicle [1 % methyl-cellulose (MC); n = 5] from 2 days before bile duct ligation (BDL). Mice were then randomly assigned to BDL or sham-operated groups (SO; n = 5). For the BDL groups, the common bile duct was exposed and ligated. Sham-operated mice underwent the same procedure with bile duct exposure but without ligation. Surgery was performed under anesthesia and sterile surgical conditions. After 48 h from the BDL procedure, mice were sacrificed, and blood and bile collected and organs harvested and snap frozen for RNA extraction and subsequent analysis. On the last day, 4 h prior the sacrifice mice were given the last oral gavage with either 1 % MC or TC-100 and subjected to fasting.

2.3. Serum analysis

Blood was obtained from the heart of anesthetized mice and centrifuged at 10,000*g* for 5 min at 4°C to separate serum. Total bilirubin was measured using Diazyme kits (Diazyme, Poway, CA), following the manufacturer's instructions.

2.4. Histology

Ileal specimens were fixed in 10 % formalin (24 h), dehydrated, embedded in paraffin and subsequently stained with hematoxylin and eosin (H&E) and Periodic acid-Schiff (PAS), according to manufacturer's instructions. Stained slides were scanned on an AperioScanScope AT and image analysis and quantification was performed using AperioImageScope software (Leica Biosystems, Nußloch, Germany). PAS signal was normalized to area and image analyses were done using Aperio algorithms (Leica Biosystems). Goblet cells were also counted. Depletion of goblet cells was scored using a semiquantitative scoring index from 0 to 4 (0 = no depletion; 1 =0–10 % depletion; 2 = 10–25 % depletion; 3 = 25–50 % depletion; 4 = 50–100 % depletion; values were normalized to the SO condition). Analysis was performed by an investigator blinded to study design with results confirmed by an independent investigator.

2.5. mRNA extraction and quantitative real time qRT-PCR analysis

RNA was isolated from the liver and ileum of mice using the RNeasy Micro kit (Qiagen, Milano, Italy). cDNA was generated from 4 μg total RNA using High-Capacity DNA Archive Kit (Applied Biosystem, Foster City, CA) and following the manufacturer's instructions. Primers to

detect the *mRNA* expression level of each gene were designed using Primer Express software (Applied Biosystem) based on GenBank sequence data. *mRNA* expression levels were quantified by qRT-PCR using Power Sybr Green chemistry and normalized to cyclophilin *mRNA* levels. Validated primers for qRT-PCR used are listed in Supplementary Table 1.

2.6. Bile acid analysis

Serum and bile BAs were quantified using a Ultra Performance Liquid Chromatography-Mass Spectrometry system (UPLC-MS^2, Acquity H-Class Bio UPLC from Waters). A mixture of internal standards (6-Ethyl Cholic Acid and Tauro-6-Ethyl Cholic Acid) in methanol were added to the biological samples with a final concentration of 2.5 μM. 5 μL of sample were injected into the UPLC-ESI-MS^2 system. The UPLC is coupled to a XEVO TQD (Waters) triple quadrupole mass spectrometer, operating with negative ionization electrospray. BAs acquisition was performed in Multiple Reaction Monitoring mode (MRM). The analytical column was a UPLC CSH Phenyl-Hexyl Column (Waters) 1.7 μm, 2.1 × 75 mm protected by a guard column (Waters) 2.1 × 5 mm. The mobile phase was a mixture of ammonium acetate buffer 15 mM, pH 8.0 (Solvent A) and Acetonitrile: Methanol = 75:25(V/V) (Solvent B). The analysis was performed in the gradient mode. Elution was performed at a flow rate of 0.44 mL/min. Sample injection volume was 5 μL. The temperature of the chromatographic column was maintained at 45 °C.

2.7. Serum extraction method

100-μL aliquots of serum samples were spiked with 10 μL of the internal standards working solution and were diluted. Serum samples were loaded onto the conditioned SPE (The solid phase extraction, C18) cartridge and then eluted with 3 mL of methanol. The eluate was dried under vacuum and then reconstituted with 100 μL of the mobile phase (ammonium acetate buffer: acetonitrile = 50:50 v/v), and injected into the UPLC-ES-MS system.

2.8. Bile extraction method

Mouse bile samples were brought to room temperature, briefly stirred, and suitably diluted with mobile phase (ammonium acetate buffer: acetonitrile = 50:50 v/v), previously spiked with the internal standards working solution. The final solution was transferred into an autosampler vial and injected into the UPLC-ES-MS system.

2.9. Prokaryotic profiling of cecal microbiome

Total DNA was extracted from 50 mg of cecal content sampled from the analyzed mice (16 mice in total, divided according to the treatment in: 6 mice for TC-100 group, 5 mice for SO group, 5 mice for MC group) using the FastDNA© SPIN Kit for Soil (BIO 101, Carlsbad, CA) following the manufacturer's instructions. The bead-beating step was performed in the FastPrep Instrument (BIO 101, Carlsbad, Canada) set to 6.0 m/s speed for 40 s. In order to check for possible contaminations related to the extraction process, negative control samples were prepared using nuclease free water and processed together with the samples. The quantity and quality of the extracted DNA were assessed using the NanoDrod 2000c (Thermo Fisher Scientific, Inc., DE, USA) and agarose gel (1 %) electrophoresis, respectively. The V5–V6 hypervariable regions of the bacterial 16S rRNA genes were chosen as the target for Prokaryotic identification [40]. The total DNA extracted from each sample was used as template for amplicon libraries preparation following the protocol described in [41]. The obtained metagenomic libraries were sequenced by the MiSeq platform (Illumina) and generated 2 × 250 paired-end (PE) reads, using the V2 chemistry. The phage PhiX genomic DNA library was added to the mix and co-sequenced as internal control for Illumina sequencing run. Raw sequences were analyzed by using the QIIME2 pipeline (version 2019.7; https://qiime2.org/) [42] relying on the ASVs (Amplicon Sequence Variants) inference and their taxonomic classification. In particular, PE sequences were imported and the Illumina adapters removed by using cutadapt. Following the evaluation of sequence quality, the PE were denoised by the DADA2 plugin [43]. During this step, the specific V5–V6 primer pairs were trimmed and the raw reads filtered according to the observed expected error. Then, he obtained ASVs were taxonomically annotated by using the feature-classifier (method: classify_sklearn) plugin [44] against Silva database (release 138) [45]. The phylogenetic inference was achieved by using the align-to-tree-mafft-fasttree plugin: a multiple sequence alignment of ASVs sequences was obtained by using MAFFT [46] and the phylogenetic tree was inferred by the maximum-likelihood procedure implemented in Fasttree 2 [47]. Contaminant ASVs were identified and removed by using the R package Decontam [48]. According to rarefaction curves, the ASV table was normalized by rarefaction to 115,000 sequences per sample and alpha and beta diversity analysis were performed, using the diversity core-metrics-phylogenetic plugin.

In order to investigate putative metabolic functions of the bacterial communities associated with the investigated samples, the metagenomic prediction tool called "Phylogenetic Investigation of Communities by Reconstruction of Unobserved States 2" (PICRUSt2, version 2.2.0-b [49], was applied. The ASV data, generated from QIIME2, were used as input for the analysis.

The microbial network was obtained by applying the Weighted Gene Correlation Network Analysis (WGCNA) R package [50], on genera aggregated counts. Initially, the clr (centered log-ration) transformation was applied to the ASVs table, to properly address the compositional nature of DNA-metabarcoding data [51]. To reduce the effect of spurious associations and highlight strong correlations, a Spearman correlation matrix was inferred and transformed into a weighted adjacency one by WGCNA. In particular, the adjacency matrix was obtained by raising the absolute correlation by a soft thresholding power β, which was empirically determined by considering the lowest power obtaining a scale-free topology index (R^2) of 0.80. The adjacency matrix was transformed into a topological overlap matrix, to optimally reduce the effect of spurious correlation, and dissimilarities were calculated. Finally, highly co-occurrent genera were clustered in modules by using a minimum size of 5. Module associations with serum and bile BAs were measured by Spearman rank correlation (r_s). Modules with p values $\leq$ 0.05 were regarded as significant. The microbial network was plotted by using the R package graph and considering only edges with an association strength $\geq$ 0.2.

2.10. Absolute quantification of Akkermansia muciniphila

Droplet digital PCR (ddPCR) (Bio-Rad, CA, USA) was performed to quantify the *A. muciniphila* 16S rRNA gene copy number in the tested samples. The ddPCR reaction mixtures were prepared on ice by mixing 11 μL of 2 × QX200TM ddPCR EvaGreen Supermix (Bio-Rad), 200 nM of *A. muciniphila* specific primers pair [52] and 1 μL of the DNA extracted from cecal samples at different concentration (100, 10, 1, 0.1 and 0.01 ng). Emulsion was produced in the QX200 Droplet Generator (Bio-Rad) according to the manufacturer's instructions. Thermal cycling conditions were as follows: 1 cycle at 95 °C for 5 min, 40 cycles at 95 °C for 30 s and 60 °C for 1 min, 1 cycle at 4 °C for 5 min, 1 cycle at 90 °C for 5 min, final hold at 4 °C. Each DNA sample was analyzed at least in duplicate, preparing independent dilutions. For each experiment, a negative control (no template control) was used. Absolute quantification was performed using QuantaSoft software (Bio-Rad, CA, USA, version 7.4.1) and the negative/positive thresholds were manually set, excluding samples with a number of droplets lower than 10,000. Output results were expressed in 16S copies/mg of cecal content. For each analyzed sample, the obtained results were converted to number of copies present in the starting material, taking into consideration the 3 copies of the 16S rRNA

gene present in *A. muciniphila*.

2.11. Statistical analysis

All results are expressed as means ± standard error of the mean (SEM). Statistically significance traits in the microbial composition characterizing the analyzed samples were evaluated at different taxonomic ranks using both ANOVA univariate and LDA effect size (LEfSe) methods [53]. Moreover, the statistical comparisons among the microbial taxa and pathway abundances were performed by using the ANCOM-BC package, which is specifically designed to deal with compositional data and controls for False Discovery Rate by correcting p-values using the Benjamini and Hochberg (BH) algorithm [54]. Statistical analyses for all other measurements were performed with GraphPad Prism software (v5.0; GraphPad Software Inc., San Diego, CA), as indicated in figure legend.

3. Results

3.1. TC-100-dependent FXR activation protects from intestinal mucosal injury caused by BDL

Bile duct ligation induced jaundice, as indicated by increased serum total bilirubin, effect that was counteracted by TC-100 (Supplementary

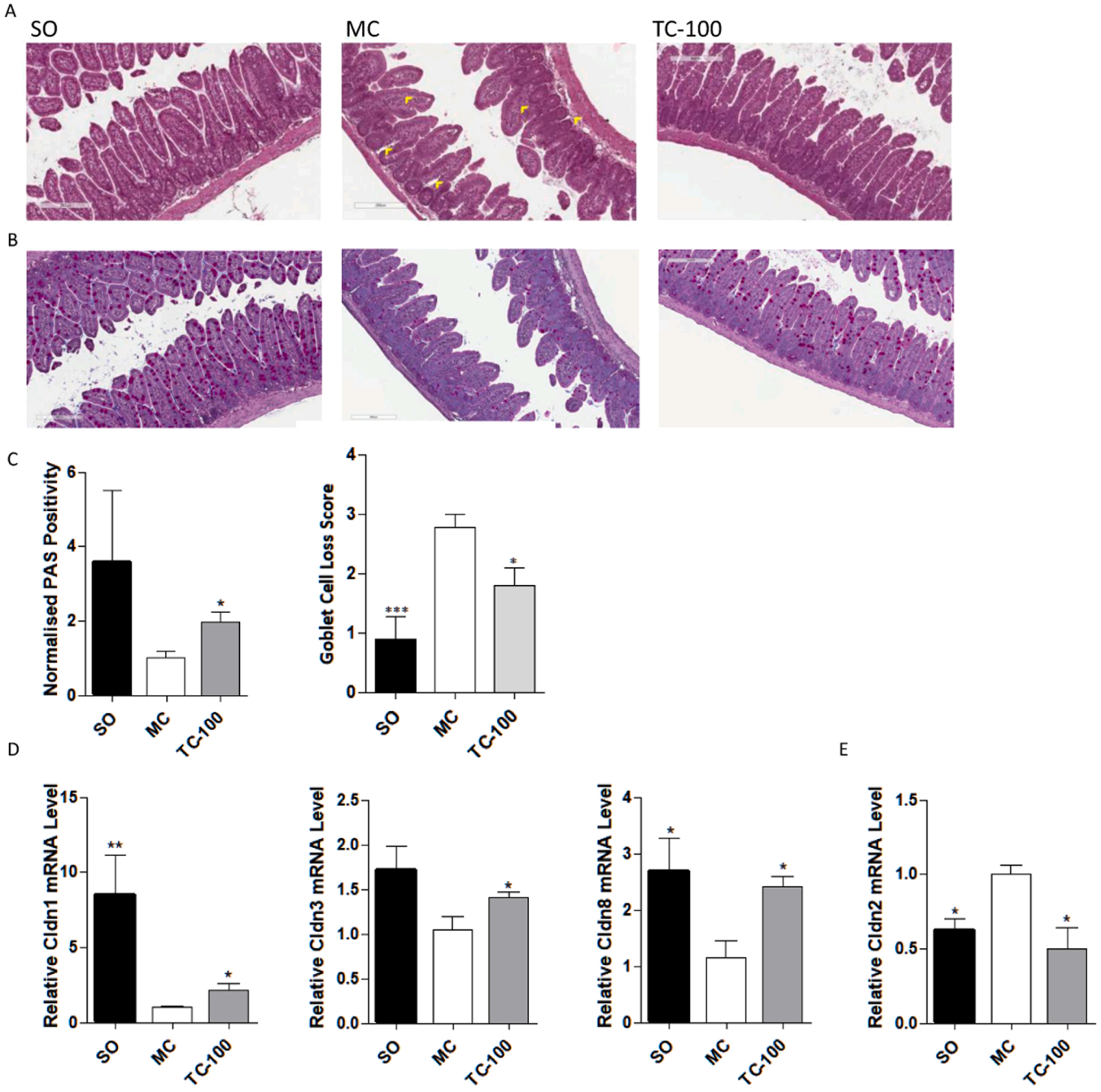

Fig. 1. TC-100-dependent FXR activation protects BDL mice from intestinal mucosa injury. Representative sections of the terminal ileum are shown for SO mice, and BDL mice treated with vehicle (MC) and TC-100. Sections were stained with H&E (A) and PAS (B). Edema is indicated by yellow arrowheads (scale bar 200 μm) (A). Quantification of PAS positivity (C) and Goblet cell loss score. Quantitative real time qRT-PCR of Cldn-1, Cldn-2, Cldn-8 (D) and Cldn-2 (E). Statistical analysis was performed using ANOVA followed by Dunnett's post hoc test (*$p < 0.05$ vs MC, ***$p < 0.001$ vs MC).

Fig. 1). To assess whether lack of BAs due to BDL caused intestinal mucosal damage and the potential effects of TC-100 in this respect, ileal section were stained with H&E and PAS, which detects mucosubstances and mucins in tissues. BDL caused an early stage submucosal edema and Goblet cell loss, that were prevented by TC-100-dependent FXR activation (Fig. 1A–C). Alterations in the expression levels of tight junctions affect the intestinal barrier integrity in different ways [55]. In particular, downregulation of claudin 1 (Cldn-1) [56], Cldn-3 [57,58] and Cldn-8 [59] can drastically reduce the barrier integrity; in contrast, claudin-2, is a tight junction protein required for the formation of paracellular water channels that and is highly expressed in leaky epithelial tissues, is upregulated in IBDs and promotes inflammation [59–61]. TC-100-dependent Fxr activation promoted the upregulation of Cldn-1, Cldn3 and Cldn-8 (Fig. 1D), while downregulating the expression of the "leaky" [62–64] Cldn2 (Fig. 1E). Taken together, these data indicate that TC-100-dependent intestinal Fxr activation protects from signs of intestinal mucosal injury in BDL mice.

3.2. TC-100 activates FXR-dependent control of BA synthesis in the gut-liver axis and decreases BA levels and hydrophobicity index in serum and bile in BDL mice

Previously published work from our group have shown that mice lacking intestinal BAs due to BDL and treated with TC-100 displayed a strong induction of the Fxr-Fgf15 duo in the gut-liver axis, ultimately controlling BAs synthesis via Cyp7a1 repression in the liver [38]. To evaluate whether this impacted BA metabolism in mice, BA pool size and composition were quantified. Serum BA composition is shown in Table 1. Mice subjected to BDL and treated with MC presented with a serum BA concentration 50-fold higher than the SO group ($p<0.001$). TC-100 administration significantly reduced the total BA pool size by 67% ($p<0.001$; Fig. 2A). Tau-CA was the most prominent primary-conjugated BA in mouse serum, followed by Tau-MCA. Both endogenous BAs were increased upon BDL. TC-100 treatment strongly decreased Tau-CA levels (331 ± 19.86 μM in MC group vs 50.96 ± 26.26 μM in TC-100-treated mice, *$p<0.05$; see Table 1, Fig. 2B). In contrast, treatment with TC-100 did not reduce levels of Tau-MCA significantly (90 ± 10 μM in MC group vs 81 ± 12 μM in TC-100-treated mice, see Table 1). Therefore, treatment with TC-100 reduced the levels of Tau-CA but not the levels of Tau-MCA which then becomes the most abundant BA in the pool of these mice (Fig. 2C). Since the relative enrichment in Tau-MCA (Fig. 2C) could reflect a change in the hydrophilicity of the BA pool, the hydrophobicity Index (HI) was calculated. TC-100 shifted the HI of the BA mixture toward lower hydrophobicity, indicating a reduced circulating toxic potential. Each BA's contribution to the overall HI is dependent on its relative abundance within the mixture, and therefore low abundance species such as deoxycholic acid (DCA), chenodeoxycholic acid (CDCA) and UDCA have lower impact. Consequently, the shift towards increased hydrophilicity is primarily driven by an increase in the relative abundance of Tau-α-MCA, a highly hydrophilic species. TC-100-treated mice clearly displayed, indeed, a more hydrophilic BA pool compared to vehicle-treated mice (Table 2 and Fig. 2D).

Endogenous BA concentration in bile samples was also quantified

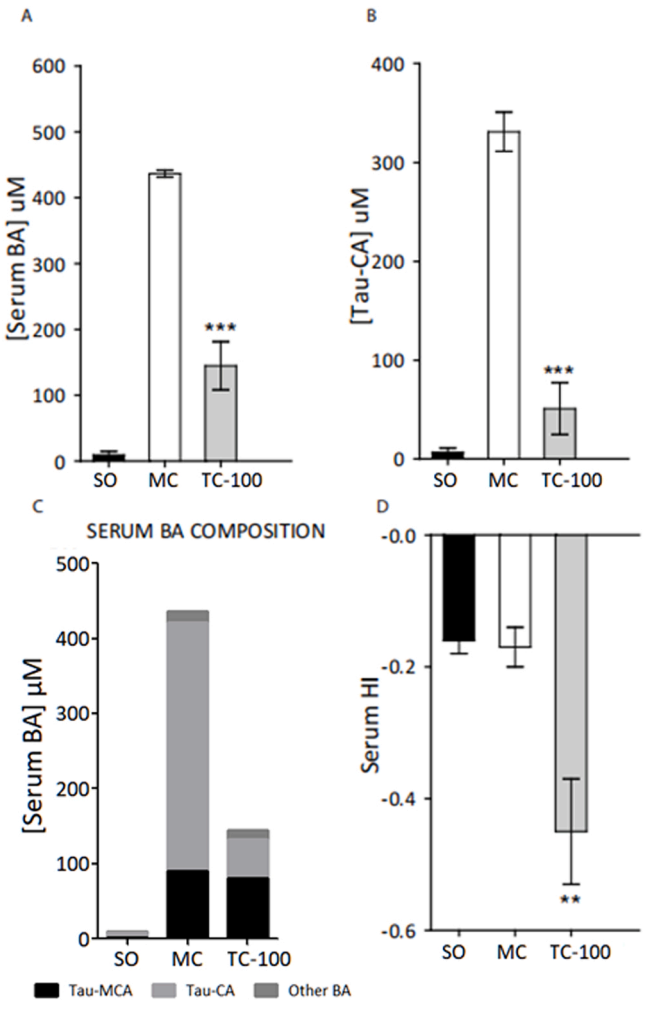

Fig. 2. TC-100-dependent FXR activation decreases serum BA pool and composition in BDL mice. Serum BA concentration (A). Quantitation of Tau-CA in serum samples (B). Endogenous serum BA pool composition (C). Graphical representation of the change in the hydrophobicity index in serum samples (D). Concentration values are expressed as mean ± SEM in μM. Statistical analysis was performed using ANOVA followed by Dunnett's post hoc test (**$p < 0.01$ vs MC; *** $p < 0.001$ vs MC).

Table 2
Serum BAs hydrophobicity index.

	Mean ± SD
SO	-0.16 ± 0.02
Vehicle	-0.17 ± 0.03
TC-100	-0.45 ± 0.08**

Statistical analysis was performed using Mann-Whitney test (TC100 vs Vehicle; **$p<0.01$).

Table 1
Endogenous serum BAs (μM).

	Tau-DCA	Tau-CDCA	DCA	CDCA	GCA	Tau-CA	Tau-UDCA	CA	UDCA	Tau-MCA	MCA	Total BA
SO	0.06 ± 0.05	0.11 ± 0.1	0.07 ± 0.03	0.03 ± 0	0.04 ± 0.03	6.79 ± 4.19	0.17 ± 0.11	0.09 ± 0.05	0.03 ± 0.02	1.91 ± 1.2	0.08 ± 0.05	9.38 ± 5.56
Vehicle	0.63 ± 0.53	4.5 ± 0.21	0.09 ± 0	0.05 ± 0.03	0.87 ± 0.29	331.2 ± 19.86	4.79 ± 4.01	0.49 ± 0.17	0.04 ± 0	89.65 ± 9.87	4.13 ± 0.41	436.3 ± 5.21
TC-100	0.21 ± 0.12	9.31 ± 2.76*	0 ± 0	0.01 ± 0*	0.07 ± 0.03*	50.96 ± 26.26*	1.03 ± 0.4*	0 ± 0**	0 ± 0	80.83 ± 12.14	2.32 ± 0.86*	144.7 ± 36.51*

Statistical analysis was performed using the Mann-Whitney test (TC100 vs Vehicle; *$p<0.05$; **$p<0.01$).

Table 3
Endogenous bile BAs (mM).

	Tau-DCA	Tau-CDCA	GCA	Tau-CA	Tau-UDCA	CA	Tau-MCA	MCA	Total BA
SO	0.35 ± 0.06	0.66 ± 0.14	0.02 ± 0.01	9.63 ± 0.2	0.53 ± 0.14	0.13 ± 0.05	7.31 ± 0.41	0.12 ± 0	18.78 ± 0.63
Vehicle	0.39 ± 0.2	0.49 ± 0.26	0.04 ± 0.02	19.9 ± 4.38	0.97 ± 0.56	0.04 ± 0.03	13.43 ± 2.92	0.09 ± 0.02	35.36 ± 4.5
TC-100	0.47 ± 0.17	0.84 ± 0.14*	0.02 ± 0*	10.8 ± 2.54**	0.59 ± 0.14	0.04 ± 0.02	12.12 ± 2.2	0.05 ± 0.02	24.94 ± 1.57**

Statistical analysis was performed using the Mann-Whitney test (TC100 vs Vehicle; *p<0.05; **p<0.01).

(Table 3). Mice subjected to BDL and treated with MC presented with double bile BA concentration compared to the surgery control group (SO; **p<0.01). In sharp contrast, treatment with TC-100 reduced bile BA concentration by 29%. (**p<0.01; Fig. 3A). Analyzing all BA species quantified in bile samples (Table 3), Tau-CA levels were significantly decreased by treatment with TC-100 (*p<0.05; Fig. 3B). TC-100 significantly reduced the total BA pool in bile of mice subjected to BDL (*p<0.05; Fig. 3C). Subsequently, the hydrophobicity index was calculated (Table 4). Despite a decrease of 29 % in hydrophobicity in mice subjected to BDL and treated with TC-100, HI changes were not significant (Fig. 3D). This is probably due to the extremely high BA concentration in bile and a slightly higher intra-variability.

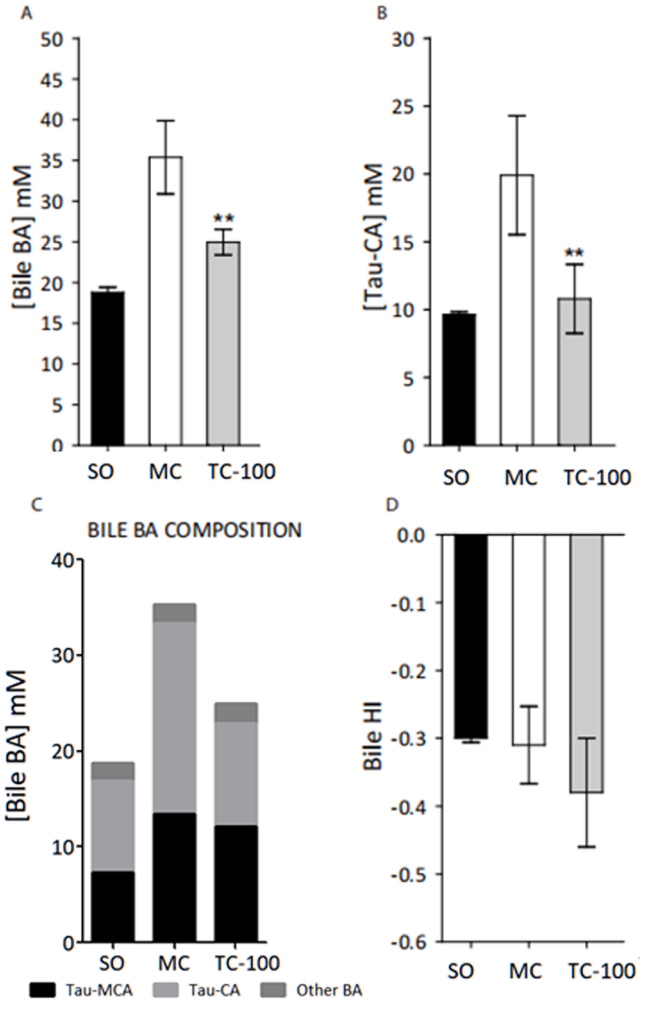

Fig. 3. TC-100-dependent FXR activation decreases bile BA pool and modifies its composition in BDL mice. BA concentration in bile (A). Quantitation of Tau-CA levels in bile sample (B). Endogenous bile BA pool composition (C). Graphical representation of the change in the hydrophobicity index in bile samples (D). Concentration values are expressed as means ± SEM in μM. Statistical analysis was performed using ANOVA followed by Dunnett's post hoc test (**p<0.01 vs MC).

Table 4
Bile BAs HI.

	Mean ± SD
SO	-0.30 ± 0.01
Vehicle	-0.31 ± 0.06
TC-100	-0.38 ± 0.08

3.3. TC-100 promotes intestinal microbiome reshaping in BDL mice and nurtures an intestinal environment favorable to Amuc enrichment in BDL mice

To explore whether the protection of the intestinal mucosa structure by TC-100 works via regulation of the GM composition in BDL mice, from each of the 16 samples a library of dual indexed 420 bp long amplicons of the V5–V6 hypervariable regions of the 16S rRNA gene were successfully sequenced, obtaining about 270.000 reads/sample. Based on the ASVs counts generated by DADA2, rarefaction curves were generated (Fig. 4A) and two alpha diversity indices calculated (Fig. 4B–C). No significant variation was observed amongst the different experimental conditions. To investigate beta diversity, weighted and unweighted UniFrac dissimilarity matrices were used to obtain Principal Coordinates Analysis (PCoA) plots (Fig. 4D–E). In the weighted UniFrac plot (Fig. 4D), all samples related to treatment with TC-100 clustered apart from SO according to the first component (PCoA1 93.27%). MC samples were proportionally distributed among the other two groups (TC-100 and SO). MC and SO samples were overall discriminated along the second component (PCoA2 2.84%). Moreover, an intra-group clustering for TC-100 was observed along the y-axis. Considering the unweighted UniFrac plot (Fig. 4E), results obtained with the weighted UniFrac analysis were confirmed and characterized by a clear separation between the treated and the other two groups, according to the first component (PCoA1 40.5%). A sub-clustering of TC-100 samples was observed on the y-axis (PCoA2 16.49%). Permanova analysis highlighted how mice groups are associated to 63% and 40% of the observed diversity using weighted and unweighted UniFrac measures, respectively (Table 5).

Taxonomic assignments and relative abundances for phylum, class and family are shown as donut charts (Fig. 5). Only the taxa with a relative abundance (RA) equal or higher than 1% were plotted, otherwise they were collapsed into "Others". Actinobacteriota, Bacteroidota, Campilobacterota, Cyanobacteria, Deferribacterota, Desulfobacterota, Firmicutes, Patescibacteriota, Proteobacteria, Verrucomicrobiota were the phyla assigned to the three conditions. Among these phyla, Bacteroidota (28.72±6.19% in the SO, 22.99±13.44% in the MC, 17.47 ±10.26% in the TC-100), Firmicutes (58.65±21.72% in the SO, 60.26 ±17.32% in the MC, 62.54±9.15% in the TC-100) and Verrucomicrobiota (1.93±1.7 % in the SO, 5.40±6.97% in the MC, 15.83±4.27% in the TC-100), were common among SO, MC and TC-100 samples (RA>1%). Statistical comparison among microbial taxa showed a statistically significant abundance of the phyla Bacteroidota and Deferribacterota in SO (p<0.05). The family *Bacteroidaceae* and genus *Bacteroides* were also more abundant in SO compared to TC-100. The Bacteroidia was the only class belonging to the phylum Bacteroiodota. The families *Bacteroidaceae, Muribaculaceae, Prevotellaceae* and *Rikenellaceae* (c. *Bacteroidia*, o. *Bacteroidales*), were identified in all the analyzed samples, represented at genus level by *Bacteroides,*

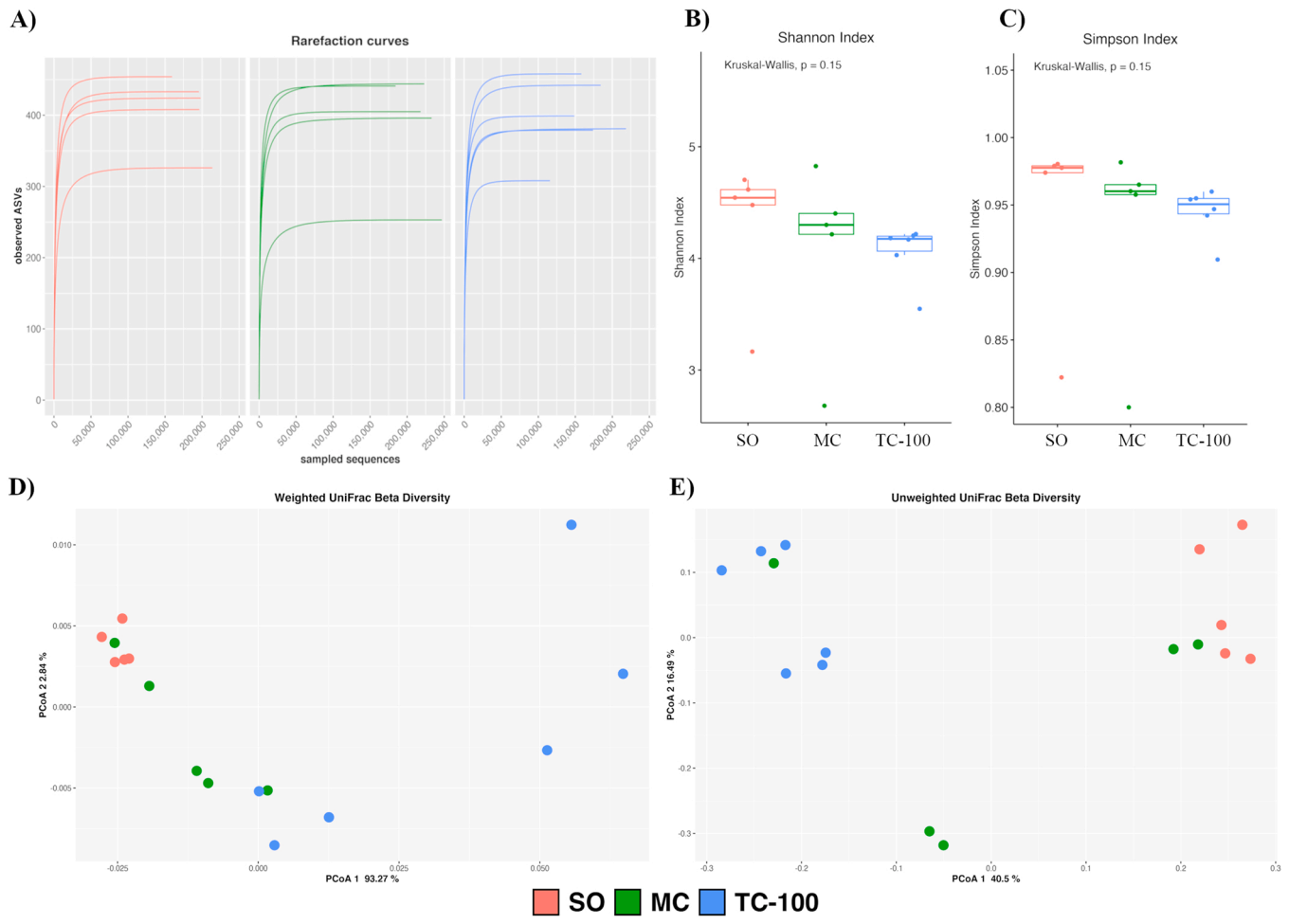

Fig. 4. No significant alpha diversity variation was observed amongst the different experimental conditions. Rarefaction curves obtained by sampling an increasing number of sequences (A). Shannon and Simpson diversity (alpha diversity) indices are shown as box-plots according to treatment groups (B–C). PCoA plots obtained for weighted and unweighted UniFrac dissimilarity matrices (D–E).

Table 5
Permanova analysis was performed by using both weighted and unweighted UniFrac distances. R^2 and p-values represent the portion of data variability explained by the proposed model and the achieved significance, respectively. Residuals correspond to the amount of variability the model was unable to capture.

	Weighted UniFrac		Unweighted UniFrac	
	R^2 (%)	P-value	R^2 (%)	P-value
Conditions	63.07	0.001	40.24	0.001
Residuals	36.03		59.76	

Muribaculaceae, Muribaculum, Prevotella and *Alistipes*, respectively. At species level the *Bacteroides caecimuris* was significantly more abundant in SO compared to TC-100 samples ($p<0.05$). The *Prevotellaceae NK3B31 group* was statistically more abundant in TC-100 compared to SO and MC ($p<0.05$), while the genus *Muribaculum* was less abundant in TC-100 compared to SO ($p<0.05$). *Bacteroides acidifaciens* was the only species assigned, with RA>1%, in SO, MC and TC-100 (1.84±1.52%, 2.22±2.20%, 1.54±1.16%, respectively). The phylum Firmicutes was represented by the following two classes: Bacilli and Clostridia (10.06 ±5.32% in SO, 14.95±13.14% in MC, 7.53±3.67% in TC-100; 48.59 ±22.82% in SO, 45.31±29.38% in MC, 55.00±9.35% in TC-100, respectively). In the class of Bacilli, the order Lactobacillales, represented by the family *Lactobacillaceae* and genus *Lactobacillus*, were identified in all three conditions (1.97±1.41% in SO, 12.09±12.13% in MC, 5.59±3.38% in TC-100). The genus *Lactobacillus* was statistically less abundant in SO compared to TC-100 and MC conditions ($p<0.05$). The genus *Enterococcus* (o. Lactobacillales, f. *Enterococcaceae*) resulted assigned, with RA> 1%, to MC samples (3.84±7.15%). Conversely, the order Erysipelotrichales, represented by the family *Erysipelotrichaceae,* was statistically more observed in SO. In particular, the species *Ileibacterium valens* was found, with RA > 1 %, exclusively in SO ($p<0.001$). Moreover, the *Clostridium cocleatum* was more observed in SO compared to both MC and TC-100 ($p<0.001$). Within the class Clostridia, the families *Lachnospiraceae* (order *i*), *Oscillospiraceae* (o. Oscillospirales) and *Ruminococcaceae* (o. Oscillospirales) were identified. *Akkermansia muciniphila* (p. Verrucomicrobiota, o. Verrucomicrobiales, f. *Akkermansiaceae*) resulted the only assigned species (1.93 ±1.73% in SO, 5.40±6.97% in MC, 15.83±4.27% in TC-100) for the class Verrucomicrobiae, and significantly more observed in samples from TC-100-treated mice ($p<0.05$). Within the phylum Actinobacteriota, *Bifidobacterium pseudolongum* (0.17±0.24% in SO, 0.23 ±0.32% in MC, 2.36±5.17% in TC-100), and Patescibacteriota, represented by the genus *Candidatus Saccharimonas* (0.02±0.03% in SO, 0.40 ±0.45% in MC, 0.90±0.75% in TC-100), RA threshold was above 1% only in the TC-100 group. For Proteobacteria (f. *Enterobacteriaceae*), RA>1% were observed for SO and MC but not for TC-100. The other phyla were represented with relative abundance lower than 1% in all analyzed samples (Supplementary Table 2 and all the data relative to differential abundance analysis with ANCOM-BC are available in Supplementary Table 3).

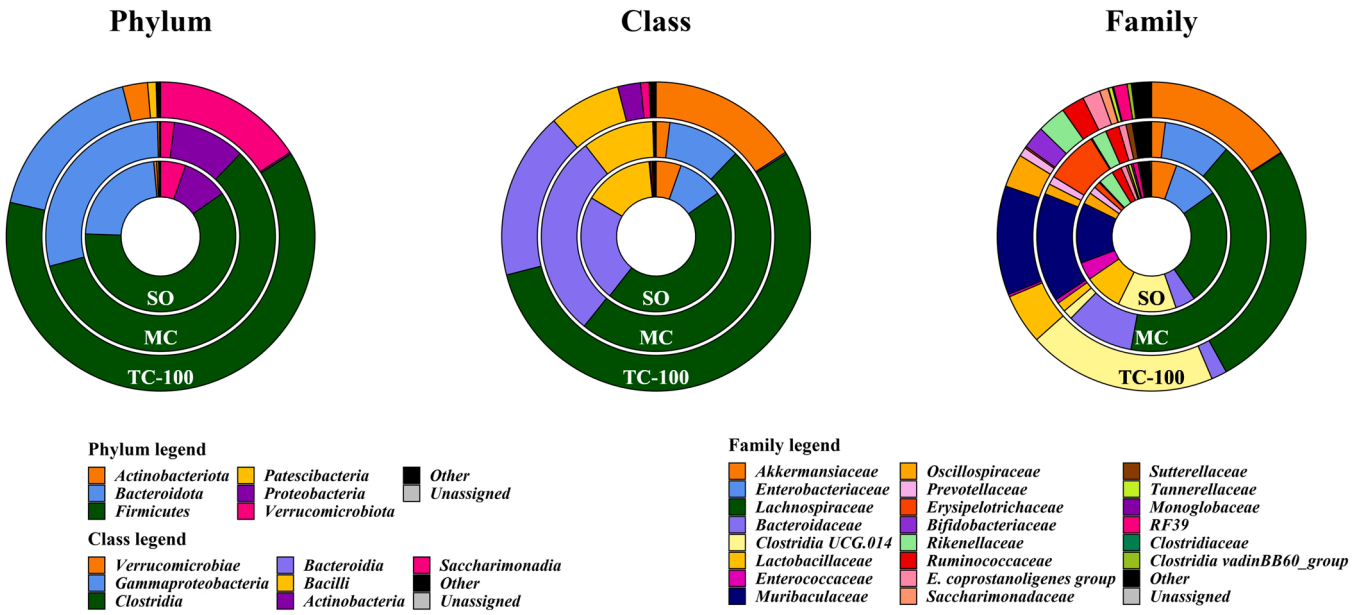

Fig. 5. Taxonomic assignments and relative abundances for phylum, class and family are shown as donut charts.

Moving on to species level, Lefse analysis have shown that *Ileibacterium valens*, *Clostridium cocleatum* and *Bacteroides caecimuris* were strongly associated to SO samples (LDA score= 3.5, 2.5 and 2.9, respectively); *Clostridiales bacterium* and *Lactobacillus murinus* were associated to MC (LDA score = 2.9 and 3.9, respectively); while, in *Akkermansia muciniphila, Parabacteroides distasonis* and *Helicobacter typhlonius* were associated to TC-100 (LDA scores = 4.1, 2.6 and 2.3, respectively) (Supplementary Table 4 and Fig. 6). Moreover, LEfSe analysis highlighted 1, 20 and 17 metabolic pathways (Supplementary Table 5 and Fig. 7) associated with MC, SO and TC-100, respectively. In particular, 14 out of 17 metabolic pathways linked to TC-100 encompassed biosynthetic activities, such as thiazole and peptidoglycan biosynthesis (LDA Score $\geq$ 3). In contrast, a catabolic signature was related to SO samples, such as adenosine nucleotides degradation and glucose degradation (LDA Score $\geq$ 3), even if also some biosynthetic activities were observed, like L-phenylalanine and L-tyrosine biosynthesis (LDA score $\geq$ 3). Only the allantoin degradation pathway was associated with MC samples (LDA Score < 3).

Akkermansia muciniphila (*Amuc*) showed the highest association in terms of Lefse with TC-100 treatment. To validate this taxonomic result in the experimental samples, absolute quantification was performed using the Droplet Digital PCR system. The copy number counts of *Amuc* resulted significantly higher in TC-100-treated mice (mean 91.419 ±7.210) compared to SO (mean 6.527±37,479, $p<0.01$) and MC treated mice (mean 27.868±25.467, $p< 0.05$) (Fig. 8).

In order to explore a possible link between highly related taxa and physiopathological read-outs in terms of BA pool composition in the different experimental groups, microbial networks were inferred by using WGCNA and highly co-occurrent nodes were clustered in 6 modules (i.e. clusters of highly correlated ASVs), collecting all the observed ASVs labeled using color names (Table 6).

The association among the WGCNA inferred clusters and serum and bile BAs were calculated. Both the Pink and Brown (r_s 0.6) modules positively correlated with the serum level of CA while red, green, and yellow showed a negative correlation (r_s − 0.6, − 0.7 and − 0.6, respectively) (Fig. 9 A). The green module positively correlated with bile levels of Tau-CDCA (r_s 0.5) while the brown one showed a negative correlation (r_s − 0.5) (Fig. 9B). Moreover, the blue module was negatively correlated with GCA (r_s − 0.5), Tau-CA (r_s − 0.5) and total BA (r_s − 0.6). The pink cluster was positively associated to both Tau-CA and total BA (r_s − 0.5). The microbial network in Supplementary Fig. 2 shows ASVs that in the previous analysis (modules) obtained a significant correlation with BA species (Supplementary Table 6). The pink nodes are mainly connected to the brown ones and each other. Yellow nodes are strictly connected to the green one, while both the green and the brown vertices represent a connection among the green and pink ones. In the green and yellow clusters several ASVs were associated to classes abundant in the TC-100 treatment group (as shown by LEfSe analysis), such as *Candidatus Saccharimonas*, *Clostridia UCG-014*, *Akkermansia*, *Helicobacter* and *Desulfovibrio*. ASVs classified as *Clostridium_senso_stricto_1*, *Faecalibaculum* and *Prevotella* were observed in the pink modules and associated to MC in LEfSe. Moreover, in the red module, the ASVs belonging to the *Monoglobus* genus is associated to MC class (as shown in LEfSe analysis).

4. Discussion

The intestinal barrier is mainly composed by the enterocyte strictly associated to each other. Its paracellular permeability is tightly regulated thanks to the coordinated activity of several tight junction proteins [65]. Destruction of the intestinal barrier cause increased intestinal permeability, which in turn disrupt intestinal homeostasis and allows translocation of pathogens or harmful substances to the blood stream. BAs are metabolites playing both a major lipid digestive role and acting as signaling molecules via the nuclear receptor FXR. FXR detects nutritional cues, thereby activating a transcriptional program involved in BA metabolic regulation. Biliary obstruction causes mucosal damage and dysbiosis in the small intestine, a detrimental event reversible by administration of BAs [19–24]. Intestinal bacteria and BAs have a mutual sophisticated relationship. In particular, BAs flowing along the intestine control bacterial overgrowth and protect against intestinal mucosal damage while intestinal microorganisms affect BA metabolism. This, in turn, shapes the magnitude of BA-induced FXR activation in the gut [24–29]. It has been previously shown that BA-dependent FXR activation protects from inflammation-driven mucosal injury in the intestine in a multilevel fashion [14]. Moreover, FGF19 administration to mice subjected to chemically-induced intestinal inflammation causes a beneficial shift in the intestinal microbiota, only in the presence of Fxr [25].

In the present study, we wanted to assess the potential enteroprotective role of the novel FXR agonist TC-100 in the absence of bile flow, hence in a condition of deactivated BA-dependent communication

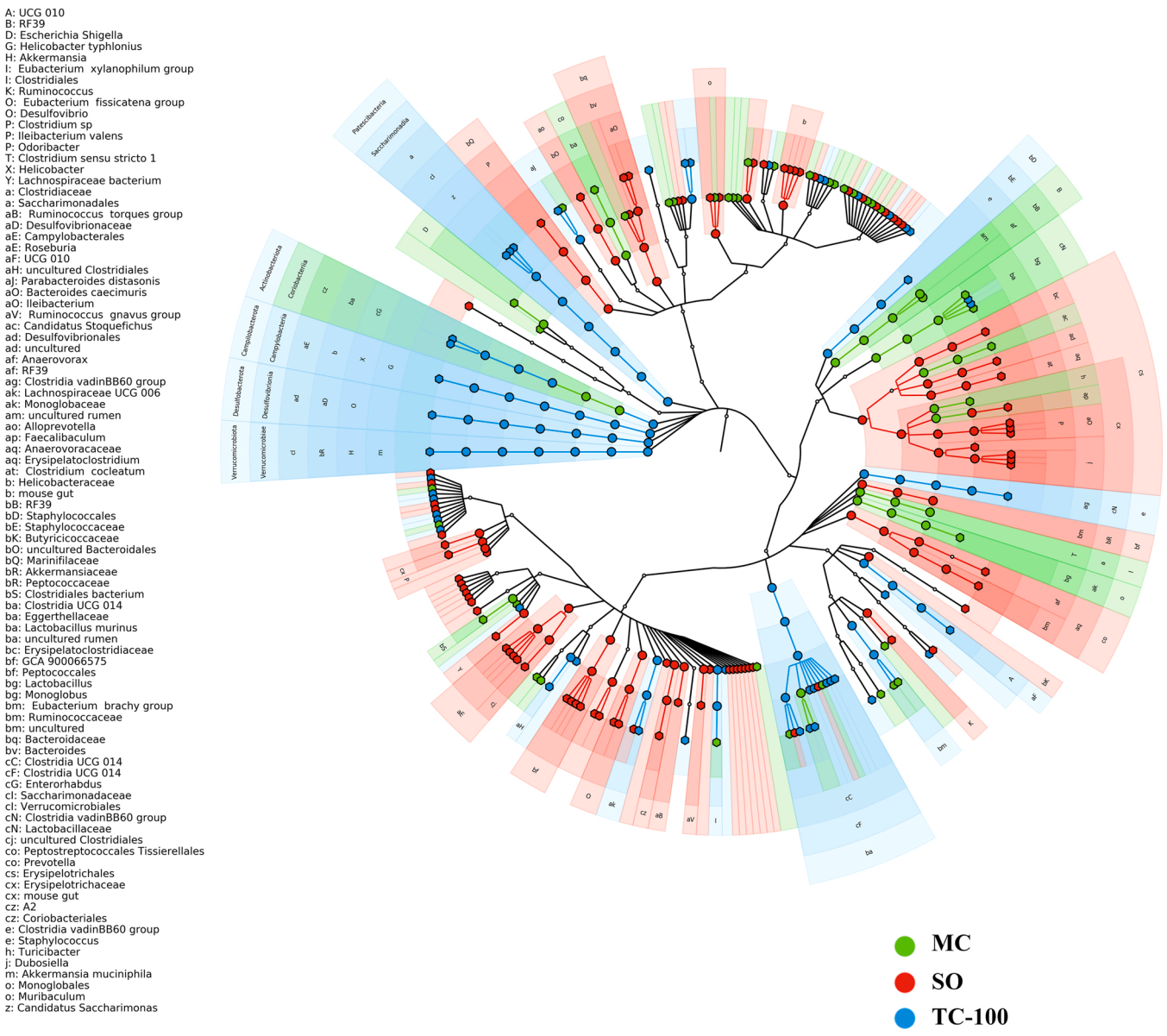

Fig. 6. Cladogram representing LEfSe results. In particular, the nodes' background reflects taxonomic association to one given condition.

between the liver and intestine. TC-100 displays intestinal compartmentalization, no chemical cytotoxicity and modulates intestinal FXR-dependent genes more effectively than OCA [38]. TC-100 is well absorbed in the intestine and metabolized as tauro-conjugate. As previously shown, TC-100-dependent FXR activation induces Fgf15 expression which in turn inhibits hepatic Cyp7a1 [38]. Here, we show that the activation of the Fxr-Fgf15 duo in the gut-liver axis decreased the BA pool size and shifts its composition to a less hydrophobic one in both serum and bile.

In the intestine, TC-100 preserves the intestinal mucosal fitness by preventing early signs of submucosal edema and Goblet cell loss due to BDL. This is accompanied by a decreased expression of the "leaky" junction Cld-2 and an increase of the "tight" junctions Cldn-1, Cldn-3 and Cldn-8. In terms of microbial signature, TC-100 shapes a different microbial population sustaining beneficial effects compared to control mice. In fact, despite an intra-sample (alpha) biodiversity statistically comparable amongst groups, beta diversity and taxonomic analyses highlight a specific microbiome signature strictly associated with each experimental condition. At phylum level, a particularly high relative abundance of Verrucomicrobiota was assessed in samples treated with TC-100. Moving onto class and then family, this translates into a higher relative abundance of Verrucomicrobiae and Akkermansiaceae. Further analysis at species level showed that Amuc had the highest association to TC-100 treatment in terms of Lefse. The remarkable enrichment of Amuc in TC-100 treated BDL mice and the concomitant preservation of the integrity of the intestinal epithelial barrier further strengthen the notion of its beneficial involvement in intestinal fitness [66,67]. Amuc belongs to the phylum Verrucomicrobia and is a Gram-negative bacterium firstly isolated in human fecal samples. This species represents 3–5% of the microbial composition in the healthy human intestinal tract [68,69] and has a central role in the regulation of the gut barrier function [70]. Amuc encodes several mucin-degrading enzymes allowing for mucus colonization and degradation resulting in the production of metabolites such as short-chain fatty acids, which play a beneficial role in metabolic health and inflammation [71,72]. It has been recently shown in a rodent model that Amuc treatment ameliorate chemically-induced mucosal inflammation potentially via promoting eubiosis while improving gut barrier functions [73]. Interestingly, Amuc has also been described as a regulator of the immune system leading to production of antimicrobial peptides and improves gut homeostasis [74,75]. Reduced levels of Amuc

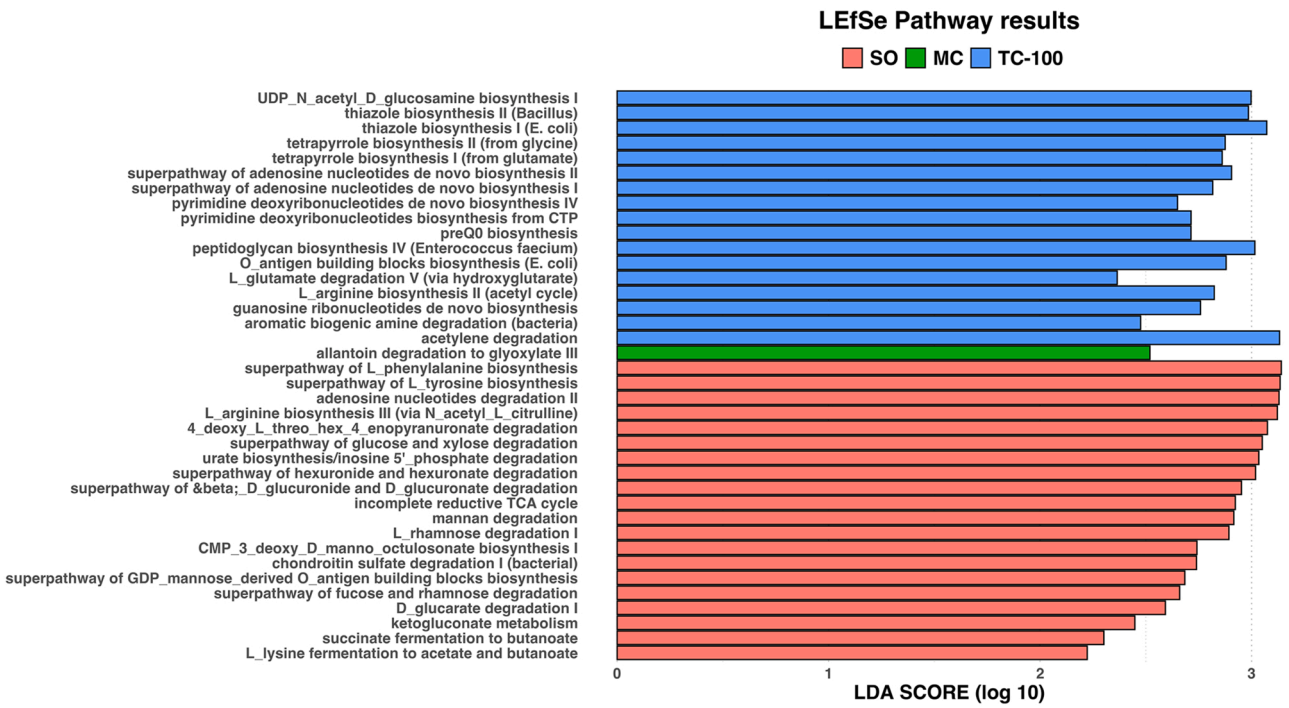

Fig. 7. Bar-plot representing LEfSe results on the inferred microbial metabolic pathways.

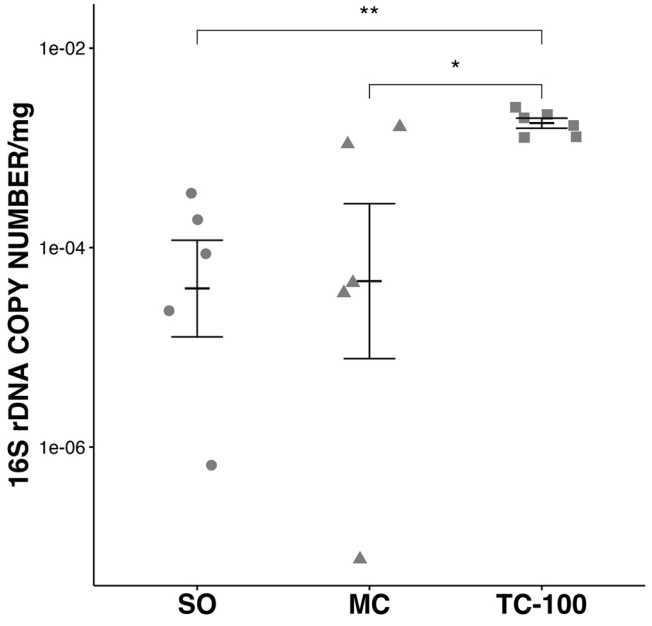

Fig. 8. ***Amuc is enriched in BLD mice treated with TC-100***. Average copy number of *Amuc* in 1 mg of cecal content collected from the different groups (SO, MC and TC-100) as determined by Droplet Digital PCR (*p<0.05, ** p<0.01).

have been observed in patients with inflammatory bowel diseases, mainly ulcerative colitis [7–76] indicating it bears anti-inflammatory properties.

To unfold the complexity of BA metabolism, the GM-BAs axis and its impact in health and disease is being actively studied and Amuc appears to be highly involved in this axis and the network data presented in this study represent a first step towards understanding the intertwined relation between microbiota species and the mice "bileome". It has been previously shown that administration of ursodeoxycholic acid could

Table 6
WGCNA modules and the corresponding number of clustered genera.

Module name	Number of clustered genera
pink	206
blue	58
brown	46
yellow	41
green	36
red	32

increase the number of Amuc and improve colitis in mice [77]. Increase in the BA pool size, and particularly CA, reduces the abundance of *Amuc* in diet–induced obese mice [78]. Moreover, primary BAs (e.g. CA, GCA, and GCDCA) have an inhibitory effect against Amuc and high BA concentration inhibits its growth in vitro [79]. In line with this, here we show for the first time that BDL-induced intestinal epithelial damage, accompanied by the increase of plasmatic primary conjugated BAs, was counteracted by TC-100. Remarkably, this is paralleled by a gut microbial reshaping characterized by an increased abundance of Amuc, which – in turn – is negatively correlated to serum CA levels.

Taken together, our data show that, in the absence of bile flow, the activation of intestinal FXR by the novel agonist TC-100 regulates BA metabolism in the gut-liver axis and nurtures an intestinal environment favorable to *Amuc* enrichment, thereby preserving the intestinal mucosa structure while contributing to the beneficial modulation of the BA pool size and composition. These findings confirm the crucial role for activated FXR in protecting the small intestine from epithelial disruption and dysbiosis and provide further evidence for the modulation of the gut microbiota by BAs. Recent findings have indicated that suppression of endogenous BA synthesis by the BA-derived drug OCA leads to an increased representation of BA–sensitive bacterial species in the human small intestine via an FXR-dependent dynamics [80]. The specific pattern of gut microbiome components associated to a specific BA profile presented here emphasizes the importance of both components as co-metabolic assets in the same organism. The mirroring of the two profiles implies the intriguing possibility of harnessing BA composition

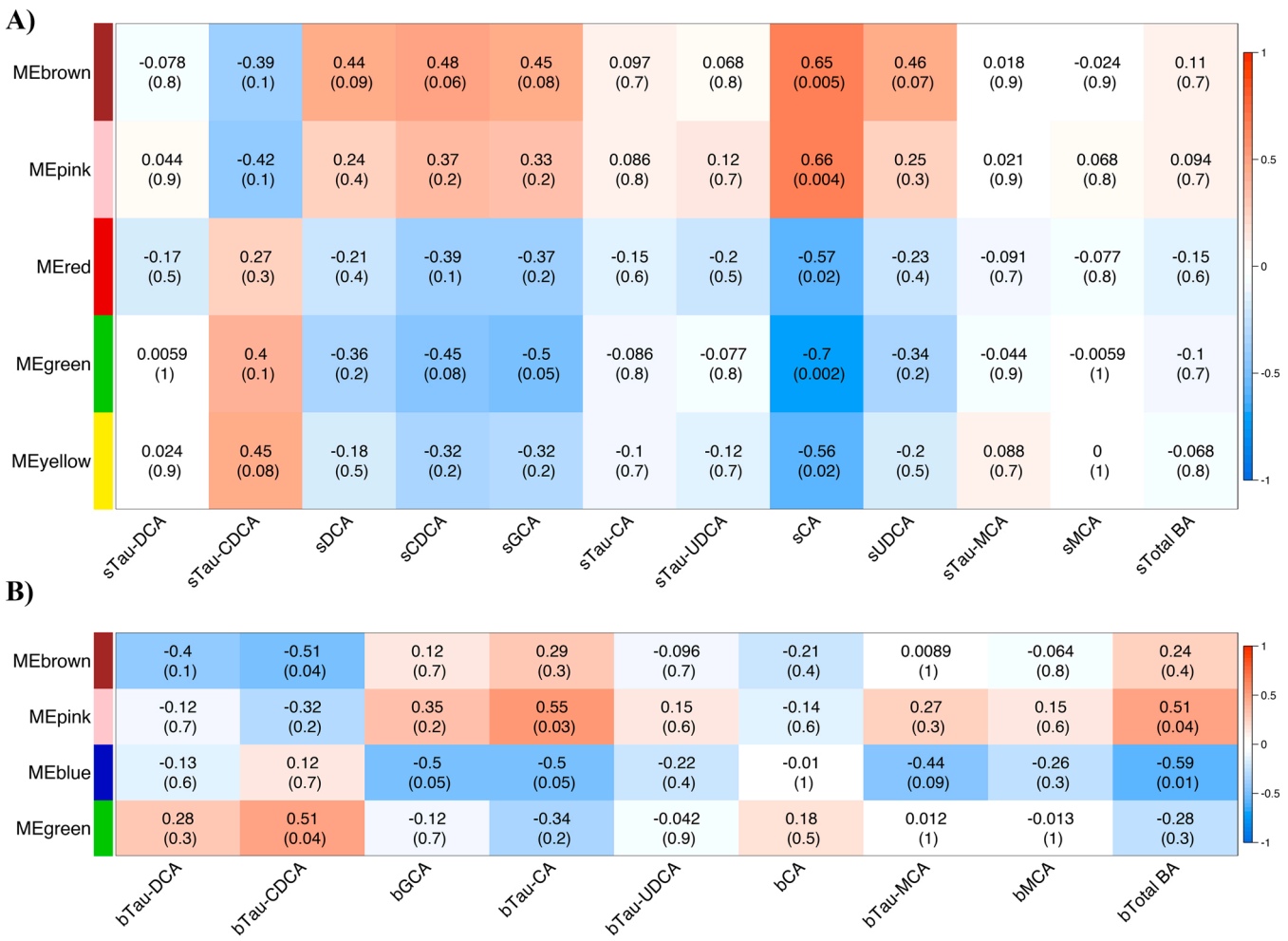

Fig. 9. Microbial and bileome networks. Association matrix between clustered genera (modules) and serum BAs. The observed modules are represented in rows and the plasma BAs in columns. Each cell contains the inferred correlation and *p*-values. Blue and red color shades correspond to negative and positive correlations, respectively (A). Associations matrix between clustered genera (modules) and bile BAs. The observed modules are represented by row and the bile BA by column. Each cell contains the inferred correlation and *p*-values. Blue and red color shades correspond to negative and positive correlations, respectively (B). Letter "s" and "b" before the different BA species indicate "serum" and "bile", respectively.

to produce an effect on the gut microbiome (and vice versa) for a healthy gut. Further research is needed to translate our findings on the beneficial role of TC-100-dependent FXR activation in maintaining the intestinal barrier integrity while promoting microbial reshaping in humans and to unravel whether Amuc could have preventive health benefits and/or represent a probiotic-adjuvant therapeutic strategy for the treatment of intestinal inflammatory diseases. Finally, the strong association between specific BA profiles and gut bacterial species needs to be further investigated to discover novel biomarkers predicting clinical response to BA-based drugs and aiding patients' stratification in diseases of the gut-liver axis, such as NASH - in which OCA has been shown to improve histological feature of fibrosis [81–83] - and intestinal inflammation concomitant to impaired bile flow, as seen in IBD-PSC patients.

Funding

This work was supported by AIRC IG 2019 23239 to AM, EU-JPI HDL-INTIMIC–MIUR FATMAL to AM and MIUR-PRIN 2017 n. 2017J3E2W2 to AM and GP.

Declaration of Interest

CC and DP are employers of TES Pharma. RP is president and CEO of TES pharma. RP and AG are cofounders of TES Pharma. All other authors have declared no conflict of interest.

Data Availability

Data available on the public repository SRA (BioProject PRJNA815965) and will be available upon publication here: https://dataview.ncbi.nlm.nih.gov/object/PRJNA815965?reviewer=k19aek6gh6bf1k3c7kb2k5e311.

Acknowledgement

We thank Dr. Claudia Peres for assistance in histopathological analysis of murine tissue samples.

Data Sharing Statement

Raw data were generated at Institute of Biomembranes, Bioenergetics and Molecular Biotechnology (IBIOM), National Council of Research (CNR), Via Amendola, 70126 Bari, Italy. The data that support the findings of this study are openly available on the public repository SRA (BioProject PRJNA815965) and will be available upon publication of this manuscript at this link: https://dataview.ncbi.nlm.nih.gov/object/PRJNA815965?reviewer=k19aek6gh6bf1k3c7kb2k5e311.

Appendix A. Supporting information

Supplementary data associated with this article can be found in the online version at doi:10.1016/j.biopha.2022.113380.

References

[1] E. Rinninella, M. Cintoni, P. Raoul, L.R. Lopetuso, F. Scaldaferri, G. Pulcini, et al., Food components and dietary habits: keys for a healthy gut microbiota composition, Nutrients 11 (10) (2019).
[2] K.J. Pflughoeft, J. Versalovic, Human microbiome in health and disease, Annu. Rev. Pathol. 7 (2012) 99–122.
[3] N. Ohtani, N. Kawada, Role of the gut-liver axis in liver inflammation, fibrosis, and cancer: a special focus on the gut microbiota relationship, Hepatol. Commun. 3 (4) (2019) 456–470.
[4] L. Macia, A.N. Thorburn, L.C. Binge, E. Marino, K.E. Rogers, K.M. Maslowski, et al., Microbial influences on epithelial integrity and immune function as a basis for inflammatory diseases, Immunol. Rev. 245 (1) (2012) 164–176.
[5] Y. Jiao, L. Wu, N.D. Huntington, X. Zhang, Crosstalk between gut microbiota and innate immunity and its implication in autoimmune diseases, Front. Immunol. 11 (2020) 282.
[6] M. Makishima, A.Y. Okamoto, J.J. Repa, H. Tu, R.M. Learned, A. Luk, et al., Identification of a nuclear receptor for bile acids, Science 284 (5418) (1999) 1362–1365.
[7] D.J. Parks, S.G. Blanchard, R.K. Bledsoe, G. Chandra, T.G. Consler, S.A. Kliewer, et al., Bile acids: natural ligands for an orphan nuclear receptor, Science 284 (5418) (1999) 1365–1368.
[8] H. Wang, J. Chen, K. Hollister, L.C. Sowers, B.M. Forman, Endogenous bile acids are ligands for the nuclear receptor FXR/BAR, Mol. Cell 3 (5) (1999) 543–553.
[9] T. Inagaki, M. Choi, A. Moschetta, L. Peng, C.L. Cummins, J.G. McDonald, et al., Fibroblast growth factor 15 functions as an enterohepatic signal to regulate bile acid homeostasis, Cell Metab. 2 (4) (2005) 217–225.
[10] I. Kim, S.H. Ahn, T. Inagaki, M. Choi, S. Ito, G.L. Guo, et al., Differential regulation of bile acid homeostasis by the farnesoid X receptor in liver and intestine, J. Lipid Res. 48 (12) (2007) 2664–2672.
[11] B. Kong, L. Wang, J.Y. Chiang, Y. Zhang, C.D. Klaassen, G.L. Guo, Mechanism of tissue-specific farnesoid X receptor in suppressing the expression of genes in bile-acid synthesis in mice, Hepatology 56 (3) (2012) 1034–1043.
[12] Y.K. Lee, D.R. Schmidt, C.L. Cummins, M. Choi, L. Peng, Y. Zhang, et al., Liver receptor homolog-1 regulates bile acid homeostasis but is not essential for feedback regulation of bile acid synthesis, Mol. Endocrinol. 22 (6) (2008) 1345–1356.
[13] J.J. Repa, D.J. Mangelsdorf, The role of orphan nuclear receptors in the regulation of cholesterol homeostasis, Annu. Rev. Cell Dev. Biol. 16 (2000) 459–481.
[14] R.M. Gadaleta, K.J. van Erpecum, B. Oldenburg, E.C. Willemsen, W. Renooij, S. Murzilli, et al., Farnesoid X receptor activation inhibits inflammation and preserves the intestinal barrier in inflammatory bowel disease, Gut 60 (4) (2011) 463–472.
[15] R.M. Gadaleta, N. Scialpi, C. Peres, M. Cariello, B. Ko, J. Luo, et al., Suppression of hepatic bile acid synthesis by a non-tumorigenic FGF19 analogue protects mice from fibrosis and hepatocarcinogenesis, Sci. Rep. 8 (1) (2018) 17210.
[16] P. Lefebvre, B. Cariou, F. Lien, F. Kuipers, B. Staels, Role of bile acids and bile acid receptors in metabolic regulation, Physiol. Rev. 89 (1) (2009) 147–191.
[17] M.E. Patti, S.M. Houten, A.C. Bianco, R. Bernier, P.R. Larsen, J.J. Holst, et al., Serum bile acids are higher in humans with prior gastric bypass: potential contribution to improved glucose and lipid metabolism, Obesity 17 (9) (2009) 1671–1677.
[18] J.M. Ridlon, J.M. Alves, P.B. Hylemon, J.S. Bajaj, Cirrhosis, bile acids and gut microbiota: unraveling a complex relationship, Gut Microbes 4 (5) (2013) 382–387.
[19] T. Inagaki, A. Moschetta, Y.K. Lee, L. Peng, G. Zhao, M. Downes, et al., Regulation of antibacterial defense in the small intestine by the nuclear bile acid receptor, Proc. Natl. Acad. Sci. USA 103 (10) (2006) 3920–3925.
[20] R.D. Berg, Bacterial translocation from the gastrointestinal tract, Adv. Exp. Med. Biol. 473 (1999) 11–30.
[21] C.J. Cahill, Prevention of postoperative renal failure in patients with obstructive jaundice–the role of bile salts, Br. J. Surg. 70 (10) (1983) 590–595.
[22] J.W. Ding, R. Andersson, V. Soltesz, R. Willen, S. Bengmark, The role of bile and bile acids in bacterial translocation in obstructive jaundice in rats, Eur. Surg. Res. 25 (1) (1993) 11–19.
[23] H.J. Evans, V. Torrealba, C. Hudd, M. Knight, The effect of preoperative bile salt administration on postoperative renal function in patients with obstructive jaundice, Br. J. Surg. 69 (12) (1982) 706–708.
[24] V. Lorenzo-Zuniga, R. Bartoli, R. Planas, A.F. Hofmann, B. Vinado, L.R. Hagey, et al., Oral bile acids reduce bacterial overgrowth, bacterial translocation, and endotoxemia in cirrhotic rats, Hepatology 37 (3) (2003) 551–557.
[25] R.M. Gadaleta, O. Garcia-Irigoyen, M. Cariello, N. Scialpi, C. Peres, S. Vetrano, et al., Fibroblast growth factor 19 modulates intestinal microbiota and inflammation in presence of Farnesoid X Receptor, EBioMedicine 54 (2020), 102719.
[26] J.K. Nicholson, E. Holmes, J. Kinross, R. Burcelin, G. Gibson, W. Jia, et al., Host-gut microbiota metabolic interactions, Science 336 (6086) (2012) 1262–1267.
[27] J.M. Ridlon, D.J. Kang, P.B. Hylemon, Bile salt biotransformations by human intestinal bacteria, J. Lipid Res. 47 (2) (2006) 241–259.
[28] S.L. Long, C.G.M. Gahan, S.A. Joyce, Interactions between gut bacteria and bile in health and disease, Mol. Asp. Med. 56 (2017) 54–65.
[29] J.M. Ridlon, S.C. Harris, S. Bhowmik, D.J. Kang, P.B. Hylemon, Consequences of bile salt biotransformations by intestinal bacteria, Gut Microbes 7 (1) (2016) 22–39.
[30] V. Urdaneta, J. Casadesus, Interactions between bacteria and bile salts in the gastrointestinal and hepatobiliary tracts, Front. Med. 4 (2017) 163.
[31] J.M. Bateup, M.A. McConnell, H.F. Jenkinson, G.W. Tannock, Comparison of Lactobacillus strains with respect to bile salt hydrolase activity, colonization of the gastrointestinal tract, and growth rate of the murine host, Appl. Environ. Microbiol. 61 (3) (1995) 1147–1149.
[32] G. Corzo, S.E. Gilliland, Bile salt hydrolase activity of three strains of Lactobacillus acidophilus, J. Dairy Sci. 82 (3) (1999) 472–480.
[33] J. Grill, F. Schneider, J. Crociani, J. Ballongue, Purification and characterization of conjugated bile salt hydrolase from Bifidobacterium longum BB536, Appl. Environ. Microbiol. 61 (7) (1995) 2577–2582.
[34] G.B. Kim, S.H. Yi, B.H. Lee, Purification and characterization of three different types of bile salt hydrolases from Bifidobacterium strains, J. Dairy Sci. 87 (2) (2004) 258–266.
[35] H. Tanaka, H. Hashiba, J. Kok, I. Mierau, Bile salt hydrolase of Bifidobacterium longum-biochemical and genetic characterization, Appl. Environ. Microbiol. 66 (6) (2000) 2502–2512.
[36] M. Kishinaka, A. Umeda, S. Kuroki, High concentrations of conjugated bile acids inhibit bacterial growth of Clostridium perfringens and induce its extracellular cholylglycine hydrolase, Steroids 59 (8) (1994) 485–489.
[37] N. Masuda, Deconjugation of bile salts by Bacteroids and Clostridium, Microbiol. Immunol. 25 (1) (1981) 1–11.
[38] R. Pellicciari, D. Passeri, F.F. De, S. Mostarda, P. Filipponi, C. Colliva, et al., Discovery of 3alpha,7alpha,11beta-Trihydroxy-6alpha-ethyl-5beta-cholan-24-oic acid (TC-100), a novel bile acid as potent and highly selective FXR agonist for enterohepatic disorders, J. Med. Chem. 59 (19) (2016) 9201–9214.
[39] V. Massafra, R. Pellicciari, A. Gioiello, S.W.C. van Mil, Progress and challenges of selective Farnesoid X Receptor modulation, Pharm. Ther. 191 (2018) 162–177.
[40] S. Chakravorty, D. Helb, M. Burday, N. Connell, D. Alland, A detailed analysis of 16S ribosomal RNA gene segments for the diagnosis of pathogenic bacteria, J. Microbiol. Methods 69 (2) (2007) 330–339.
[41] M. Marzano, B. Fosso, C. Manzari, F. Grieco, M. Intranuovo, G. Cozzi, et al., Complexity and dynamics of the winemaking bacterial communities in berries, musts, and wines from Apulian grape cultivars through time and space, PLoS One 11 (6) (2016), e0157383.
[42] E. Bolyen, J.R. Rideout, M.R. Dillon, N.A. Bokulich, C.C. Abnet, G.A. Al-Ghalith, et al., Reproducible, interactive, scalable and extensible microbiome data science using QIIME 2, Nat. Biotechnol. 37 (8) (2019) 852–857.
[43] B.J. Callahan, P.J. McMurdie, M.J. Rosen, A.W. Han, A.J. Johnson, S.P. Holmes, DADA2: High-resolution sample inference from Illumina amplicon data, Nat. Methods 13 (7) (2016) 581–583.
[44] N.A. Bokulich, B.D. Kaehler, J.R. Rideout, M. Dillon, E. Bolyen, R. Knight, et al., Optimizing taxonomic classification of marker-gene amplicon sequences with QIIME 2's q2-feature-classifier plugin, Microbiome 6 (1) (2018) 90.
[45] E. Pruesse, C. Quast, K. Knittel, B.M. Fuchs, W. Ludwig, J. Peplies, et al., SILVA: a comprehensive online resource for quality checked and aligned ribosomal RNA sequence data compatible with ARB, Nucleic Acids Res. 35 (21) (2007) 7188–7196.
[46] K. Katoh, H. Toh, Parallelization of the MAFFT multiple sequence alignment program, Bioinformatics 26 (15) (2010) 1899–1900.
[47] M.N. Price, P.S. Dehal, A.P. Arkin, FastTree 2–approximately maximum-likelihood trees for large alignments, PLoS One 5 (3) (2010), e9490.
[48] N.M. Davis, D.M. Proctor, S.P. Holmes, D.A. Relman, B.J. Callahan, Simple statistical identification and removal of contaminant sequences in marker-gene and metagenomics data, Microbiome 6 (1) (2018) 226.
[49] G.M. Douglas, V.J. Maffei, J.R. Zaneveld, S.N. Yurgel, J.R. Brown, C.M. Taylor, et al., PICRUSt2 for prediction of metagenome functions, Nat. Biotechnol. 38 (6) (2020) 685–688.
[50] P. Langfelder, S. Horvath, WGCNA: an R package for weighted correlation network analysis, BMC Bioinform. 9 (2008) 559.
[51] G.B. Gloor, J.M. Macklaim, V. Pawlowsky-Glahn, J.J. Egozcue, Microbiome datasets are compositional: and this is not optional, Front. Microbiol. 8 (2017) 2224.
[52] N. Roshanravan, R. Mahdavi, E. Alizadeh, A. Ghavami, S.Y. Rahbar, A.N. Mesri, et al., The effects of sodium butyrate and inulin supplementation on angiotensin signaling pathway via promotion of Akkermansia muciniphila abundance in type 2 diabetes; a randomized, double-blind, placebo-controlled trial, J. Cardiovasc. Thorac. Res. 9 (4) (2017) 183–190.
[53] N. Segata, J. Izard, L. Waldron, D. Gevers, L. Miropolsky, W.S. Garrett, et al., Metagenomic biomarker discovery and explanation, Genome Biol. 12 (6) (2011) R60.
[54] H. Lin, S.D. Peddada, Analysis of compositions of microbiomes with bias correction, Nat. Commun. 11 (1) (2020) 3514.
[55] M.K. Findley, M. Koval, Regulation and roles for claudin-family tight junction proteins, IUBMB Life 61 (4) (2009) 431–437.
[56] J. Wu, C. He, J. Bu, Y. Luo, S. Yang, C. Ye, et al., Betaine attenuates LPS-induced downregulation of Occludin and Claudin-1 and restores intestinal barrier function, BMC Vet. Res. 16 (1) (2020) 75.
[57] S. Milatz, S.M. Krug, R. Rosenthal, D. Gunzel, D. Muller, J.D. Schulzke, et al., Claudin-3 acts as a sealing component of the tight junction for ions of either charge and uncharged solutes, Biochim. Biophys. Acta 1798 (11) (2010) 2048–2057.
[58] Y. Miyoshi, S. Tanabe, T. Suzuki, Cellular zinc is required for intestinal epithelial barrier maintenance via the regulation of claudin-3 and occludin expression, Am. J. Physiol. Gastrointest. Liver Physiol. 311 (1) (2016) G105–G116.

[59] S. Zeissig, N. Burgel, D. Gunzel, J. Richter, J. Mankertz, U. Wahnschaffe, et al., Changes in expression and distribution of claudin 2, 5 and 8 lead to discontinuous tight junctions and barrier dysfunction in active Crohn's disease, Gut 56 (1) (2007) 61–72.
[60] R. Ahmad, R. Chaturvedi, D. Olivares-Villagomez, T. Habib, M. Asim, P. Shivesh, et al., Targeted colonic claudin-2 expression renders resistance to epithelial injury, induces immune suppression, and protects from colitis, Mucosal Immunol. 7 (6) (2014) 1340–1353.
[61] D. Gunzel, A.S. Yu, Claudins and the modulation of tight junction permeability, Physiol. Rev. 93 (2) (2013) 525–569.
[62] S. Amasheh, N. Meiri, A.H. Gitter, T. Schoneberg, J. Mankertz, J.D. Schulzke, et al., Claudin-2 expression induces cation-selective channels in tight junctions of epithelial cells, J. Cell Sci. 115 (Pt 24) (2002) 4969–4976.
[63] R. Rosenthal, S. Milatz, S.M. Krug, B. Oelrich, J.D. Schulzke, S. Amasheh, et al., Claudin-2, a component of the tight junction, forms a paracellular water channel, J. Cell Sci. 123 (Pt 11) (2010) 1913–1921.
[64] A. Tamura, H. Hayashi, M. Imasato, Y. Yamazaki, A. Hagiwara, M. Wada, et al., Loss of claudin-15, but not claudin-2, causes Na^{+} deficiency and glucose malabsorption in mouse small intestine, Gastroenterology 140 (3) (2011) 913–923.
[65] M.C. Arrieta, L. Bistritz, J.B. Meddings, Alterations in intestinal permeability, Gut 55 (10) (2006) 1512–1520.
[66] P.D. Cani, W.M. de Vos, Next-generation beneficial microbes: the case of Akkermansia muciniphila, Front. Microbiol. 8 (2017) 1765.
[67] L. Zheng, C.J. Kelly, K.D. Battista, R. Schaefer, J.M. Lanis, E.E. Alexeev, et al., Microbial-derived butyrate promotes epithelial barrier function through IL-10 REceptor-dependent Repression of Claudin-2, J. Immunol. 199 (8) (2017) 2976–2984.
[68] C. Belzer, W.M. de Vos, Microbes inside–from diversity to function: the case of Akkermansia, ISME J. 6 (8) (2012) 1449–1458.
[69] M. Derrien, E.E. Vaughan, C.M. Plugge, W.M. de Vos, Akkermansia muciniphila gen. nov., sp. nov., a human intestinal mucin-degrading bacterium, Int. J. Syst. Evol. Microbiol. 54 (Pt 5) (2004) 1469–1476.
[70] M.C. Collado, M. Derrien, E. Isolauri, W.M. de Vos, S. Salminen, Intestinal integrity and Akkermansia muciniphila, a mucin-degrading member of the intestinal microbiota present in infants, adults, and the elderly, Appl. Environ. Microbiol. 73 (23) (2007) 7767–7770.
[71] R. Zhai, X. Xue, L. Zhang, X. Yang, L. Zhao, C. Zhang, Strain-specific anti-inflammatory properties of two Akkermansia muciniphila strains on chronic colitis in mice, Front. Cell Infect. Microbiol. 9 (2019) 239.
[72] T. Zhang, X. Ji, G. Lu, F. Zhang, The potential of Akkermansia muciniphila in inflammatory bowel disease, Appl. Microbiol. Biotechnol. 105 (14–15) (2021) 5785–5794.
[73] X. Bian, W. Wu, L. Yang, L. Lv, Q. Wang, Y. Li, et al., Administration of Akkermansia muciniphila ameliorates dextran sulfate sodium-induced ulcerative colitis in mice, Front. Microbiol. 10 (2019) 2259.
[74] M. Derrien, B.P. van, G. Hooiveld, E. Norin, M. Muller, W.M. de Vos, Modulation of mucosal immune response, tolerance, and proliferation in mice colonized by the mucin-degrader Akkermansia muciniphila, Front. Microbiol. 2 (2011) 166.
[75] C.W. Png, S.K. Linden, K.S. Gilshenan, E.G. Zoetendal, C.S. McSweeney, L.I. Sly, et al., Mucolytic bacteria with increased prevalence in IBD mucosa augment in vitro utilization of mucin by other bacteria, Am. J. Gastroenterol. 105 (11) (2010) 2420–2428.
[76] S.L. James, C.T. Christophersen, A.R. Bird, M.A. Conlon, O. Rosella, P.R. Gibson, et al., Abnormal fibre usage in UC in remission, Gut 64 (4) (2015) 562–570.
[77] L. Van den Bossche, P. Hindryckx, L. Devisscher, S. Devriese, W.S. Van, T. Holvoet, et al., Ursodeoxycholic acid and its taurine- or glycine-conjugated species reduce colitogenic dysbiosis and equally suppress experimental colitis in mice, Appl. Environ. Microbiol. 83 (7) (2017).
[78] X. Zheng, F. Huang, A. Zhao, S. Lei, Y. Zhang, G. Xie, et al., Bile acid is a significant host factor shaping the gut microbiome of diet-induced obese mice, BMC Biol. 15 (1) (2017) 120.
[79] T. Hagi, S.Y. Geerlings, B. Nijsse, C. Belzer, The effect of bile acids on the growth and global gene expression profiles in Akkermansia muciniphila, Appl. Microbiol. Biotechnol. 104 (24) (2020) 10641–10653.
[80] E.S. Friedman, Y. Li, T.D. Shen, J. Jiang, L. Chau, L. Adorini, et al., FXR-dependent modulation of the human small intestinal microbiome by the bile acid derivative obeticholic acid, Gastroenterology 155 (6) (2018) 1741–1752.
[81] B.A. Neuschwander-Tetri, R. Loomba, A.J. Sanyal, J.E. Lavine, M.L. Van Natta, M. F. Abdelmalek, et al., Farnesoid X nuclear receptor ligand obeticholic acid for non-cirrhotic, non-alcoholic steatohepatitis (FLINT): a multicentre, randomised, placebo-controlled trial, Lancet 385 (9972) (2015) 956–965.
[82] Z.M. Younossi, V. Ratziu, R. Loomba, M. Rinella, Q.M. Anstee, Z. Goodman, et al., Obeticholic acid for the treatment of non-alcoholic steatohepatitis: interim analysis from a multicentre, randomised, placebo-controlled phase 3 trial, Lancet 394 (10215) (2019) 2184–2196.
[83] Z.M. Younossi, M. Stepanova, F. Nader, R. Loomba, Q.M. Anstee, V. Ratziu, et al., Obeticholic acid impact on quality of life in patients with nonalcoholic steatohepatitis: REGENERATE 18-month interim analysis, Clin. Gastroenterol. Hepatol. (2021).